

A new electron-multiplier-tube-based beam monitor for muon monitoring at the T2K experiment

Y. Ashida^{a,*}, M. Friend^b, A. K. Ichikawa^a, T. Ishida^b, H. Kubo^a,
K. G. Nakamura^a, K. Sakashita^b, W. Uno^a

^a*Department of Physics, Kyoto University, Kyoto 606-8502, Japan*

^b*High Energy Accelerator Research Organization (KEK), Tsukuba, Ibaraki 305-0801, Japan*

Abstract

Muon beam monitoring is indispensable for indirectly monitoring accelerator-produced neutrino beams in real time. Though Si photodiodes and ionization chambers have been successfully used as muon monitors at the T2K experiment, sensors that are more radiation tolerant are desired for future operation. We have investigated the electron-multiplier tube (EMT) as a new sensor for muon monitoring. Secondary electrons produced by the passage of muons at dynodes are multiplied in the tube and produce signal. Two prototype detectors were installed at the T2K muon monitor location, and various EMT properties were studied based on in situ data taken with the T2K muon beam. The signal size is as expected based on calculation, and the EMTs show a sufficiently fast time response for bunch-by-bunch beam monitoring. The spill-by-spill intensity resolution is 0.4%, better than the required value (1%). Signal linearity within $\pm 1\%$ is achieved at proton beam powers up to 460 kW (with +250 kA focusing horn operation). A gradual signal decrease was observed during the initial exposure, due to the stabilization of dynode materials, before the response became stable within $\pm 1\%$. This work demonstrates that EMTs are a good candidate for future muon monitoring at T2K, and may also have other more general applications.

1. Introduction

With the steady increase of beam power at high-intensity beam facilities, as well as the push for higher precision measurements, the importance of beam monitoring is growing, both to protect equipment, and to precisely measure beam properties. A beam intensity can span many orders of magnitude, from one to 10^{13} particles per hundred nanoseconds. Counting detectors are applicable when the intensity is up to order $10^7/\text{s}$, but do not work at higher intensities. Rather, current-mode read-out is used at these higher intensities. When the number of charged particles exceeds around $10^{15}/\text{s}$, a secondary emission monitor, the signal of which is an electrical current produced by the radiation-induced emission of secondary electrons from a conductor foil, has sufficiently large signal for 50- Ω -load read-out. For intermediate intensities still too high for particle counting, detectors utilizing ionization or excitation of media, such as semiconductors, scintillators, and gases, are used.

*Corresponding author

Email address: assy@scphys.kyoto-u.ac.jp (Y. Ashida)

For accelerator neutrino beam experiments, monitoring the muons produced along with neutrinos has played a key role in beam control (see Refs. [1, 2] and references therein). Ionization detectors and Si photodiodes have been used at the T2K experiment, where the typical number of muons is around $10^{12}/\text{s}$. However, during the recent high-intensity operation, as described in Section 2, the radiation damage of Si sensors and signal saturation of ionization detectors started to become issues.

In this paper, we report the investigation of the electron-multiplier tube, or EMT, which is equivalent to a photomultiplier tube (PMT) without a photocathode, as a new muon monitor for the T2K experiment. This is the first ever study of beam monitoring using EMTs at the intensity level of 10^6 particles per hundred nanoseconds. After a description of the T2K muon monitor and its current status in Section 2, we describe the principle of muon monitoring using electron-multiplier tubes in Section 3 and our EMT prototype sensors in Section 4. Then, we report the initial performance test results obtained with the muon beam at the T2K muon monitor location in Section 5, followed by the conclusion in Section 6.

2. The muon monitor for the T2K experiment

2.1. The T2K experiment and J-PARC neutrino beamline

The T2K experiment measures neutrino oscillation parameters precisely using accelerator-produced (anti-)neutrinos [3]. A muon neutrino or anti-neutrino beam is produced at the Japan Proton Accelerator Research Complex (J-PARC) and then measured at the Super-Kamiokande (SK) detector [4], which is located 295 km from J-PARC. By measuring the disappearance of muon (anti-)neutrinos and the appearance of electron (anti-)neutrinos, T2K determines the neutrino oscillation parameters and probes CP violation in the lepton sector [5, 6].

A 30 GeV proton beam from the main ring (MR) synchrotron of J-PARC impinges on a graphite target to produce predominantly pions and some fraction of kaons. The generated particles are parallel-focused by three magnetic horns [7, 8], currently operated at positive or negative 250 kA, in order to focus positively or negatively charged outgoing particles, respectively. The hadrons then decay into neutrinos and muons in a 96-m-long decay volume, producing a neutrino beam or an anti-neutrino beam depending on the focusing horn polarity. Both the direction and intensity of the neutrino beam must be known precisely in order to precisely predict the neutrino flux at SK. The neutrino beam profile spreads as wide as a few km at SK, but a 1 mrad change in the direction of the beam axis causes a significant change in the neutrino event rate and a distortion of the energy spectrum, which leads to large systematic errors on the neutrino flux. Near detectors sit 280 m downstream of the target to monitor the beam direction and intensity, as well as to study neutrino-nucleus interactions. One of the near detectors, INGRID, is composed of 14 modules arranged in a cross spanning $10\text{ m} \times 10\text{ m}$ around the beam center axis, and monitors the neutrino beam direction and intensity by measuring the event rate at each module [9]. The INGRID detector gives direct information about the neutrino beam properties, however, it requires more than one day to accumulate sufficient data for a neutrino beam profile measurement because of the small interaction cross section of neutrinos. On the other hand, as explained below, the T2K muon monitor can reconstruct the beam profile for each beam bunch.

The neutrino beam direction is affected by various sources, i.e. the position of the proton beam at the target, misalignment of the target or horns, etc. In each 2.48 s beam cycle, a

proton beam spill composed of eight bunches, which are separated by 581 ns and typically have an 80 ns bunch width (3σ), is extracted to the neutrino beamline. Bunch-by-bunch beam monitoring is indispensable for primary proton beam tuning and diagnostics of the proton beam and beamline equipment. The proton beam intensity is monitored by five current transformers (CT), and the position and profile of the proton beam are measured by nineteen segmented secondary emission monitors (SSEM). In this paper, we use the values measured by the most downstream monitors, CT5, SSEM18, and SSEM19. The fluctuation of the CT relative intensity measurement is as small as 0.5%. In addition to the proton beam monitors, T2K has a muon monitor, which monitors the profile and intensity of the muons produced along with the neutrinos. The muon monitor sits 118 m away from the target, downstream of a beam dump, at the end of the T2K decay volume. The target, horns, and first part of the beam dump, which is made of graphite blocks, are in a vessel filled with helium gas. The second part of the beam dump is downstream of the He vessel and is composed of concrete blocks. This is followed by the muon monitor, which also sits outside the helium vessel. The beam dump thickness is designed such that only muons with momentum higher than 5 GeV penetrate it, while hadrons and low-momentum muons are absorbed. These monitors give bunch-by-bunch information and have been used for proton beam tuning and alignment checks of the target, horns, and baffle located upstream of the target. Figure 1 shows a schematic drawing of the beamline equipment from the most downstream part of the primary beamline to the muon monitor.

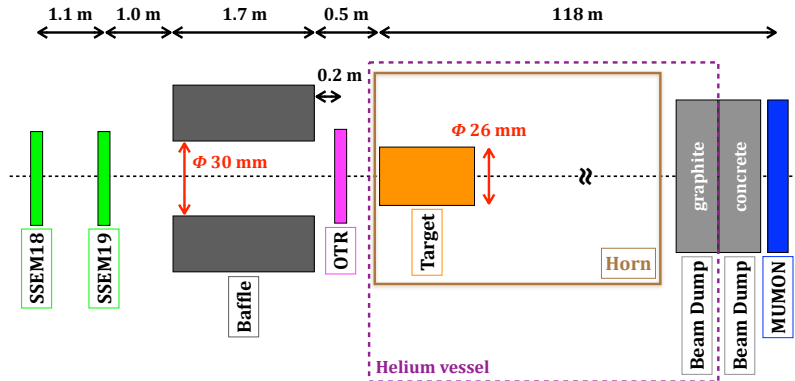


Figure 1: Schematic drawing of the neutrino beamline equipment from the most downstream part of the primary proton beamline to the muon monitor. Though an optical transition radiation monitor (OTR) [10] is placed just before the target, its information is not used in this analysis.

2.2. The T2K muon monitor (MUMON)

The current muon monitor (MUMON) system is composed of two arrays of sensors, one of silicon PIN photodiodes (Si; HAMAMATSU[®] S3590-08) and another of ionization chambers (IC; Ar+N₂ or He+N₂) [11], where the Si array sits upstream of the IC array. Each array covers a 150×150 cm² region that has 7×7 channels installed with a 25 cm pitch. A schematic view of the MUMON is shown in Figure 2. Seventy-meter-long polyimide cables for signal and high voltage are drawn from the underground muon monitor location to an electronics hut on the ground. The sensor waveforms are stored in a 65 MHz flash analog-to-digital converter

(ADC) in the COmmon Pipelined Platform for Electronics Readout (COPPER) system [12]. At high-intensity beam operation, additional attenuation modules are used to attenuate the signal size to be within the flash ADC dynamic range. The precision (systematic uncertainty) of the MUMON beam direction measurement is 0.28 mrad and the resolution is better than 0.03 mrad [13]. During beam operation, the MUMON continuously monitors the muon beam profile and intensity, and if any major deviation from the expected muon beam profile is measured an alarm is issued and the proton beam is tuned. The system has been working well since the beginning of the T2K experiment. When the horn current is set to +250 kA (neutrino beam mode), the muon flux at the MUMON is 1.09×10^5 /cm²/10¹² POT (protons on target). At 485 kW proton beam power (the present maximum power), the muon flux is 3.5×10^6 /cm² per 80 ns beam bunch. For -250 kA (anti-neutrino beam mode), the muon flux becomes about two-thirds of that at +250 kA, due to the difference in the focused pion flux.

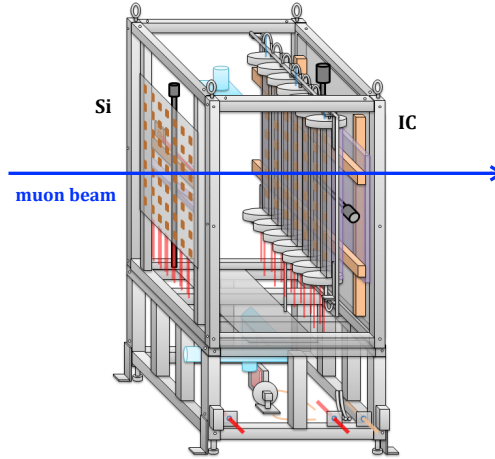


Figure 2: Schematic view of the T2K muon monitor [11]. Each array of Si and IC sensors covers a 150×150 cm² region with 7×7 channels.

2.3. Concerns for the current muon monitors

There is a plan to increase the J-PARC beam power up to 1.3 MW from 485 kW and the horn current to 320 kA from 250 kA [14]. At the 1.3 MW operation phase, a 1.16 s beam cycle is planned, where the number of beam bunches becomes nearly doubled. In this situation, the averaged muon flux is expected to become about three times larger than the current flux, and the flux for the beam bunch is 4.9×10^6 /cm² per 80 ns beam bunch. Under such a large muon flux irradiation, we expect certain issues with the current muon monitors, some of which have already been observed even at the present muon flux.

The Si sensors will suffer radiation damage, and monthly regular replacements may be necessary. Figure 3 shows the evolution of the ratio of the total yield of the Si and IC (Ar gas) sensors over several J-PARC operation periods. By taking the ratio of the two, fluctuations from other sources, such as the proton beam condition or horn current, are canceled. The ratio decreased by 1.2% after irradiation of about 7×10^{20} POT at +250 kA horn current (7.82×10^{13} /cm² integrated protons). The fact that the IC yield was stable within $\pm 0.2\%$

during that period indicates that the Si sensors themselves show signal degradation due to radiation damage.

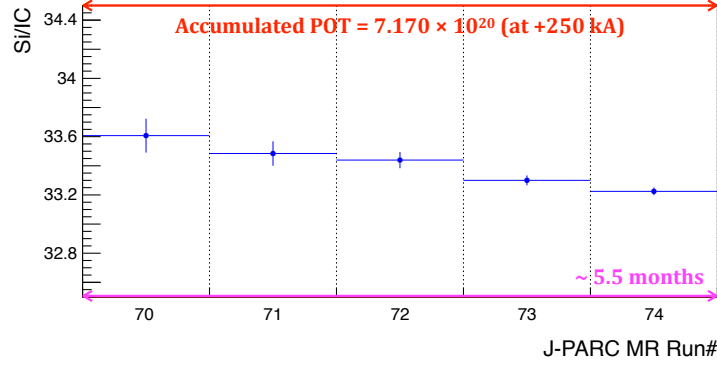


Figure 3: Ratio of the average yield of Si over IC (Ar) over the period of several MR runs with +250 kA horn current. A 1.2% decrease is seen after an accumulated POT of 7×10^{20} .

For the ionization chambers, non-linear signal response due to space charge effects becomes an issue at high intensity. When many electrons and ions are generated, the electric field is distorted by accumulated ions, which affects the signal yield. This effect appears more severely at the latter bunches because more ions are accumulated. The left panel of Figure 4 shows the IC (Ar) yield for the eighth bunch at various beam powers (all at +250 kA horn current), and indicates that non-linearities appear at 400 kW (with a muon flux of 2.9×10^6 /cm² per 80 ns beam bunch). The right panel shows the IC yield divided by the Si yield for each bunch, and a drop in the ratio is clearly seen for the final bunch. Here, the beam power and horn current are 460 kW and +250 kA, respectively. There are three potential solutions to this problem. One would be to increase the applied high voltage so that generated ions are swept out faster; however, there is a risk of reaching the chamber breakdown voltage. Another solution would be to use a lighter gas, such as He, in which the number of generated electron/ion pairs is much smaller than Ar, and therefore less charge accumulation would occur. However, lighter gases can suffer from signal pileup caused by the fast drift speed of the lighter ions, as shown in Figure 5 for He, which can affect bunch-by-bunch monitoring. Another lighter noble gas under consideration is Ne; however, Ne gas is currently prohibitively expensive. Usage of a thinner gap between the electrodes could be another solution, but this would require a full replacement of the current T2K IC system.

For these reasons, a new T2K muon monitoring system is desired for future operation. electron-multiplier tubes (EMTs) are one candidate, as described below.

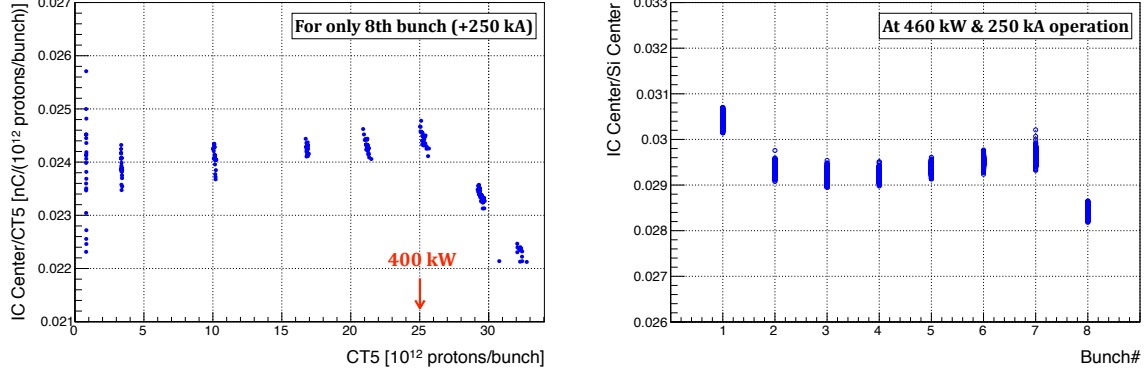


Figure 4: IC yield for the eighth bunch at various beam powers at +250 kA horn current (left) and the ratio of the IC yield to Si yield for each bunch at 460 kW and +250 kA horn current (right). The features seen in bunches 1~7 can be understood by the signal tail properties: the Si sensors have larger signals but faster decay time tails than the IC, as shown in Figure 11. The decrease in the eighth bunch is due to space charge effects in the IC.

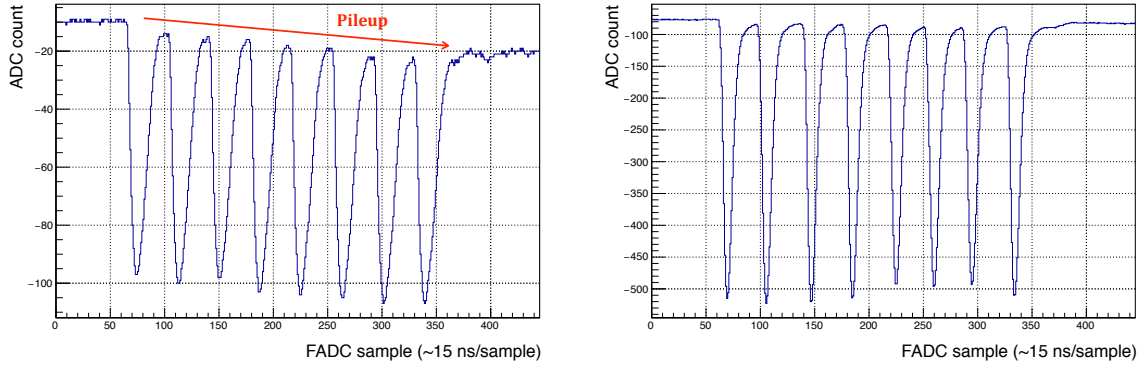


Figure 5: An example of the IC (He) signal waveform with beam power 340 kW and horn current +250 kA ($2.5 \times 10^6/\text{cm}^2$ per 80 ns beam bunch, left). For comparison, an IC (Ar) waveform with beam power 480 kW and horn current -250 kA ($2.3 \times 10^6/\text{cm}^2$ per 80 ns beam bunch, right) is shown.

3. Beam monitoring by electron-multiplier tubes

Several requirements must be satisfied when monitoring the T2K high-intensity muon beam. The signal size must be large enough to be read out without in situ electronic amplification. Fast signal response is also required for bunch-by-bunch monitoring. The device must also be radiation tolerant. Secondary electron emission monitors (SEMs) are proven to be radiation tolerant and have a fast response. However, the SEM expected signal size is too small to be used as a T2K muon monitor. Photomultiplier tubes (PMTs) use the secondary emission process to multiply electrons from the PMT photocathode. Secondary emission electrons are also produced by the passage of muons through a PMT, and the muon-induced secondary electron signal can be multiplied as usual by the PMT. For muon monitoring, however, the PMT photocathode is not necessary. Hence an electron-multiplier tube (EMT), a PMT without a photocathode, is considered as a new MUMON candidate sensor. In our study, EMTs were produced by depositing aluminum on the cathodes of PMTs. Figure 6 shows a schematic diagram of the signal multiplication by an EMT.

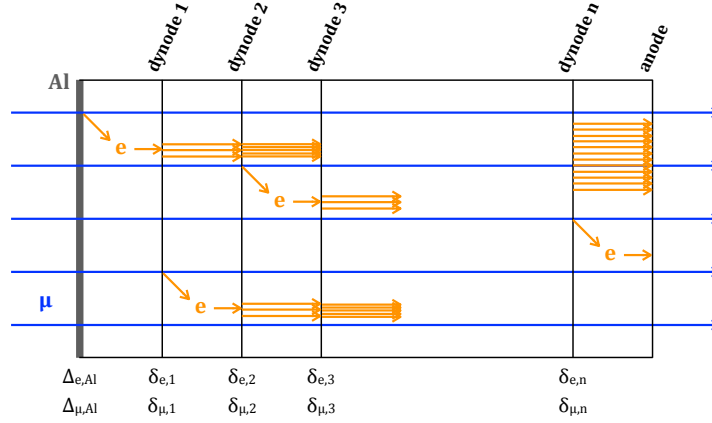


Figure 6: Schematic diagram of the signal multiplication by an electron-multiplier tube as a muon monitor. Electron- and muon-induced secondary emission occurs at the Al surface and at each dynode.

When a muon passes through the EMT, secondary electrons are produced either at the surrounding aluminum cathode or at the dynodes. The emitted electrons are accelerated, bombard the downstream dynodes, and produce more electrons. The secondary emission efficiency is defined as the number of emitted electrons divided by the number of incident particles [15], and is a characteristic of the material type, the incident particle type, and the particle energy. In Figure 6, Δ represents the secondary emission efficiency for aluminum and δ is that for dynodes. To specify the incident particle, an “e” subscript is used for electrons and a “μ” is used for muons. The dynode number is given as a subscript of δ . The secondary emission efficiency δ is dependent on the particle energy; therefore, it is possible that $\delta_{e,i}$ and $\delta_{e,j}$ ($i \neq j$) are not equal. The product of the secondary emission efficiencies of all dynodes determines the gain of the PMT:

$$G = \delta_{e,1} \times \delta_{e,2} \times \cdots \times \delta_{e,n} = \prod_{i=1}^n \delta_{e,i}. \quad (1)$$

In the case of the muon monitor, the signal is generated primarily by muons and electrons (delta-rays) knocked out by muons. The energy of the delta-rays reaches several hundred MeV [13]. These muons and delta-rays penetrate the EMT, while most of the secondary emission electrons stop once they hit the dynodes. Therefore, it is possible that secondary electrons that contribute to the signal are produced at every dynode by muons or delta-rays. The final output signal Q can be written as follows:

$$Q = Q_\mu + Q_e, \quad (2)$$

$$Q_\mu = e \cdot \phi_\mu \cdot \left\{ A_{\text{sur}} \cdot \Delta_{\mu,\text{Al}} \cdot \prod_{i=1}^n \delta_{e,i} + \sum_{i=1}^{n-1} \left(A_i \cdot \delta_{\mu,i} \cdot \prod_{j=i+1}^n \delta_{e,j} \right) \right\}, \quad (3)$$

$$Q_e = e \cdot \phi_e \cdot \left\{ A_{\text{sur}} \cdot \Delta_{e,\text{Al}} \cdot \prod_{i=1}^n \delta_{e,i} + \sum_{i=1}^{n-1} \left(A_i \cdot \delta_{e,i} \cdot \prod_{j=i+1}^n \delta_{e,j} \right) \right\}, \quad (4)$$

where e is the elementary electric charge (1.6×10^{-19} C), A_{sur} and A_i are the area of the aluminum cathode surface and each dynode surface [cm^2], respectively, and ϕ_μ (ϕ_e) is the muon (delta-ray) flux [$/\text{cm}^2$]. The first term corresponds to the secondary electron production at the aluminum cathode, and the second term to that at the i -th dynode.

As a simple case for a rough estimation, the contribution from delta-rays is ignored here and the area of each Al and dynode surface is assumed to be A . Here we assume that particles are incident on the EMT perpendicular to the surface and any change of the dynode effective surface area is not considered. In addition, the electron secondary emission efficiencies of all dynodes ($\delta_{e,i}$) are assumed to be the same (referred to as δ_e , hereafter). The typical gain of HAMAMATSU[®] R9880, which was used for the EMT studies shown here, is 5×10^3 when -500 V is applied, and the number of dynodes is $n = 10$. Therefore, the gain per dynode can be calculated as $\delta_e \sim 2.35$. The secondary emission efficiencies for muons with several GeV energy, $\Delta_{\mu,\text{Al}}$ and $\delta_{\mu,i}$, are assumed to be 0.08 [16]. The surface area is $A = 2.01 \text{ cm}^2$ (radius is 8 mm), and the normalized muon flux at horn current $+250$ kA is $\phi_\mu^{\text{normalized}} = 1.09 \times 10^5 / \text{cm}^2 / 10^{12} \text{ POT}$. Using the number of protons at beam power 460 kW, $N = 3.0 \times 10^{13} \text{ POT/bunch}$, the muon flux is calculated as $\phi_\mu = \phi_\mu^{\text{normalized}} \cdot N$. With these assumptions, the expected charge is calculated as 730 pC/bunch.

4. Prototype detectors

Two EMTs were custom-made based on the HAMAMATSU[®] metal-package PMT R9880 by depositing aluminum on the cathode. R9880 was selected due to its small footprint and short length: it is short enough to be easily installed and aligned at the muon monitor site. Figure 7 shows a photograph of the EMTC3 sensor and Figure 8 shows a schematic diagram of the divider circuit used to operate these EMTs. In Figure 8, the resistances $R_1 \sim R_{10}$ are 330 k Ω , and R_{11} is 160 k Ω , giving uniform voltage differences between the dynodes. The maximum negative high voltage applied to the cathode was limited to -500 V during our tests due to the currently installed connectors in the T2K muon monitor system. The capacitors, $C_1 \sim C_{11}$, compensate for the charge consumed on the dynodes in the process of

multiplication. To maintain linearity in the EMT response, sufficient charge, usually $100 \sim 1000$ times the consumed charge, must be stored in these capacitors [15]. The 51Ω damping resistances, R_{12} and R_{13} , are usually inserted to reduce waveform ringing, but we removed them so that the charge consumed in earlier bunches can be quickly compensated for from the capacitors.



Figure 7: A photograph of EMTC3. The monitor radius is 8 mm.

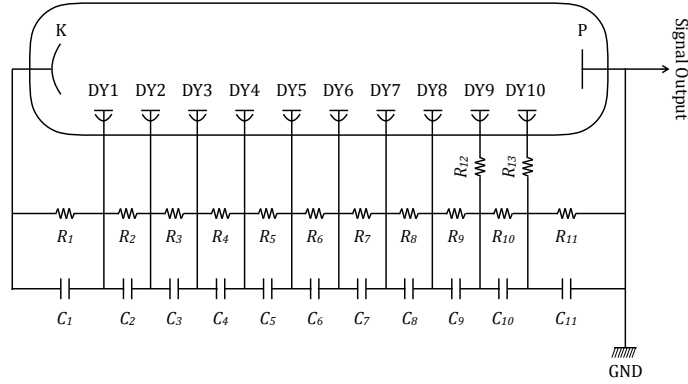


Figure 8: Schematic diagram of the divider circuit of the prototype EMT. “K”, “P”, “DY” and “GND” represent the cathode, anode, dynode, and ground, respectively. The resistances $R_1 \sim R_{10}$ are $330 \text{ k}\Omega$, and R_{11} is $160 \text{ k}\Omega$. The capacitances are given in Table 1.

We made four sets of divider circuits. The capacitances of the later versions were optimized based on initial measurement results using the earlier versions. In this paper, results of measurements with two later versions, referred to as EMTC3 and EMTC4, are reported. Table 1 summarizes the capacitances and stored charges of each capacitor used in EMTC3 and EMTC4 when a negative bias of -500 V is applied. Only C_8 to C_{11} for EMTC3 and C_6 to C_{11} for EMTC4 were used and the other capacitors were removed (represented as “-” in Table 1).

Table 1: Capacitances and stored charges for the EMTs when -500 V is applied.

	EMTC3		EMTC4	
	capacitance (nF)	charge (μC)	capacitance (nF)	charge (μC)
K-DY1 (C_1)	-	-	-	-
DY1-2 (C_2)	-	-	-	-
DY2-3 (C_3)	-	-	-	-
DY3-4 (C_4)	-	-	-	-
DY4-5 (C_5)	-	-	-	-
DY5-6 (C_6)	-	-	100	4.8
DY6-7 (C_7)	-	-	100	4.8
DY7-8 (C_8)	10	0.48	100	4.8
DY8-9 (C_9)	10	0.48	330	15.7
DY9-10 (C_{10})	10	0.48	330	15.7
DY10-GND (C_{11})	15	0.35	330	7.6

EMTC3 and EMTC4 were installed directly downstream of the T2K MUMON ionization chambers. Figure 9 shows the EMT installation positions compared with the IC sensor positions. Relative to the MUMON, the EMT sensors are vertically centered and horizontally offset from center by 26.5 cm. The signal and high-voltage cables are the same as those used for the Si and IC sensors. The read-out system is also the same; however, no attenuator module is used for the EMTs.

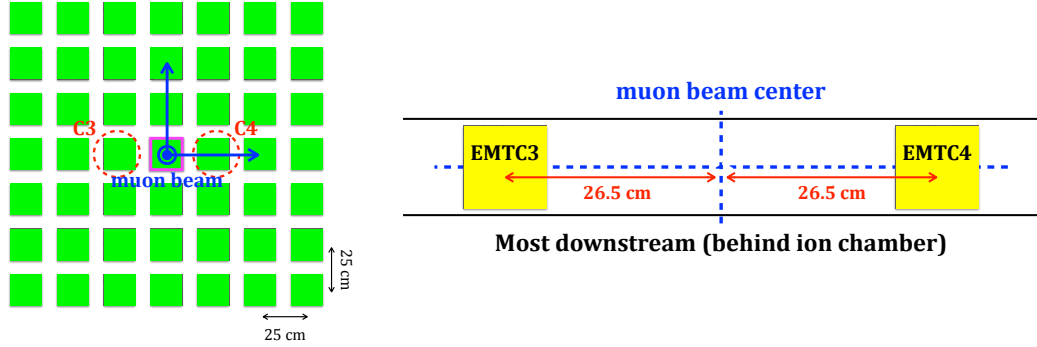


Figure 9: Prototype EMTs' horizontal and vertical installation positions overlaid with the IC sensor positions (left) and a zoom-out focusing on the geometry around the EMTs (right). Green squares in the left panel indicate the 49 channels of the ionization chambers; the one whose edge is colored magenta is the center channel.

5. Muon beam test

The performance of the EMTs (C3 and C4), including checks of the signal size, time response, intensity resolution, linearity, and stability, was studied in situ with the T2K muon beam.

5.1. Output charge

The expected output charge of an EMT was calculated in Section 3 as 730 pC/bunch at 460 kW beam power and +250 kA horn current (corresponding to a muon flux of 3.3×10^6 /cm² per 80 ns beam bunch). The measured charge output per beam bunch for EMTC3 and C4 when -500 V was applied is summarized in Table 2. Reasonable agreement with our expectation is seen. The difference in signal size between the two sensors is compatible with the expected difference between individual PMTs.

Table 2: EMT output signal size per bunch at 460 kW beam intensity and +250 kA horn current (muon flux of 3.3×10^6 /cm² per 80 ns beam bunch) with applied voltage of -500 V. The expected charge is 730 pC/bunch.

Bunch#	EMTC3 charge [pC]	EMTC4 charge [pC]
1	873.1	784.9
2	870.7	787.3
3	866.9	788.6
4	855.9	787.9
5	860.4	797.0
6	850.6	795.5
7	847.8	798.5
8	854.1	797.7
Average	859.9	792.2

5.2. Signal waveform

Figure 10 shows examples of the EMTC3 (left panel) and C4 (right panel) signal waveform. The signal has a tail component caused by both detector intrinsic properties and cable and electronics reflections. Such tails could cause the performance of bunch-by-bunch monitoring to deteriorate. To quantify the tail contribution, we calculate the ratio of the integral of the tail region to that of the first bunch signal for the EMTs, the Si center channel (Si channel at the center position of the 49 channels), and the IC center channel (IC channel at the center position of the 49 channels). The tail size is calculated by integrating the regions Tail-1 and Tail-2 shown in Figure 10, and normalizing by the signal size of the first bunch. The integration periods are the same for all three regions. The tail sizes are shown in Figure 11 when the beam power and horn current settings were 450 kW and +250 kA, respectively. It can be seen that the EMTs have a smaller tail component (about 1%) than the Si or IC sensors (a few %). Note that the tail of the eighth bunch of the IC is affected by space charge effects, as discussed in Section 2, which cause a larger tail. In the future, with higher beam intensities, this effect is expected to become more severe, since space charge effects will begin to affect earlier bunches as well. These measurements indicate that EMTs perform better than Si and IC sensors for bunch-by-bunch beam monitoring.

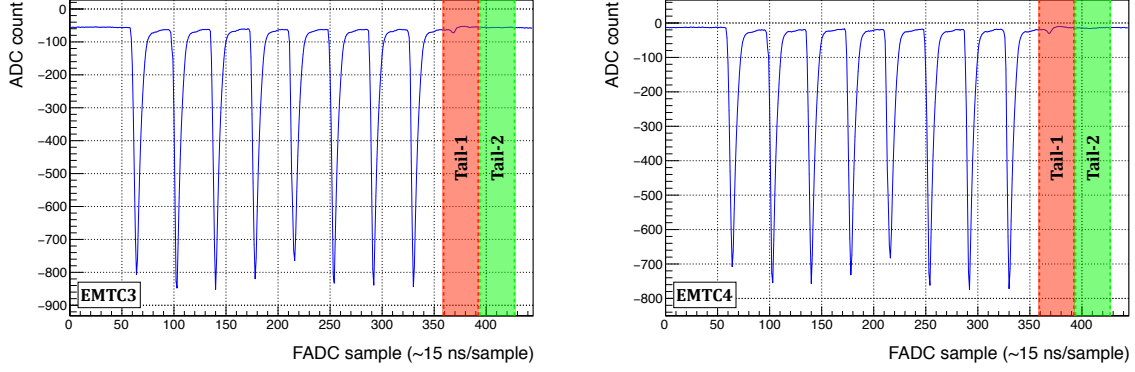


Figure 10: EMTC3 (left) and C4 (right) waveform examples. Two tail regions, Tail-1 and Tail-2, are selected to estimate the tail component contribution.

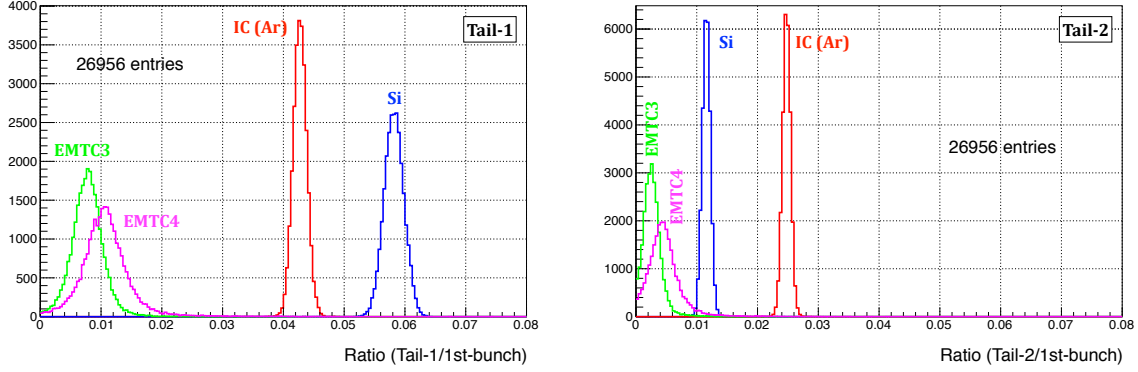


Figure 11: Tail sizes for Tail-1 (left) and Tail-2 (right). The tail integration regions are shown in Figure 10. The proton beam intensity was 450 kW and the horn current setting was +250 kA (corresponding to a muon flux of 3.2×10^6 /cm² per 80 ns beam bunch). The EMTs show a smaller tail component than the Si and IC (Ar) sensors. The Si tail component has a larger signal but faster decay time than the IC (Ar) tail.

5.3. Intensity resolution

Figure 12 shows the spill-by-spill detector signal size normalized to the proton beam intensity for the EMTs, Si center channel, and IC (Ar) center channel at a proton beam power of 450 kW and horn current of +250 kA. From these distributions, the EMT intensity resolution is calculated to be 0.34% for C3 and 0.41% for C4, while the Si and IC (Ar gas) center channels show 0.25% and 0.24% resolutions, respectively. The resolutions of each detector are summarized in Table 3, including the intensity resolution for only the first bunch. The statistical error on each value is quite small (less than 0.01%). The contribution from noise due to the read-out system including the cable, attenuator, and flash ADC was estimated by integrating the baseline pedestal before the beam spill and was found to be less than 0.1%. Compared to the current monitors, EMTs show slightly poor resolution. However, simulation studies show that a 1% uncertainty on the intensity measurement for each sensor corresponds to a 0.06 mrad uncertainty in the beam direction measurement, which is much smaller than the total precision of 0.28 mrad. In fact, the total intensity monitoring precision is limited by the calibration of the read-out system, the precision of which is a few %. Therefore, the

intensity resolution of the EMTs satisfies the requirements for muon beam direction and flux measurements.

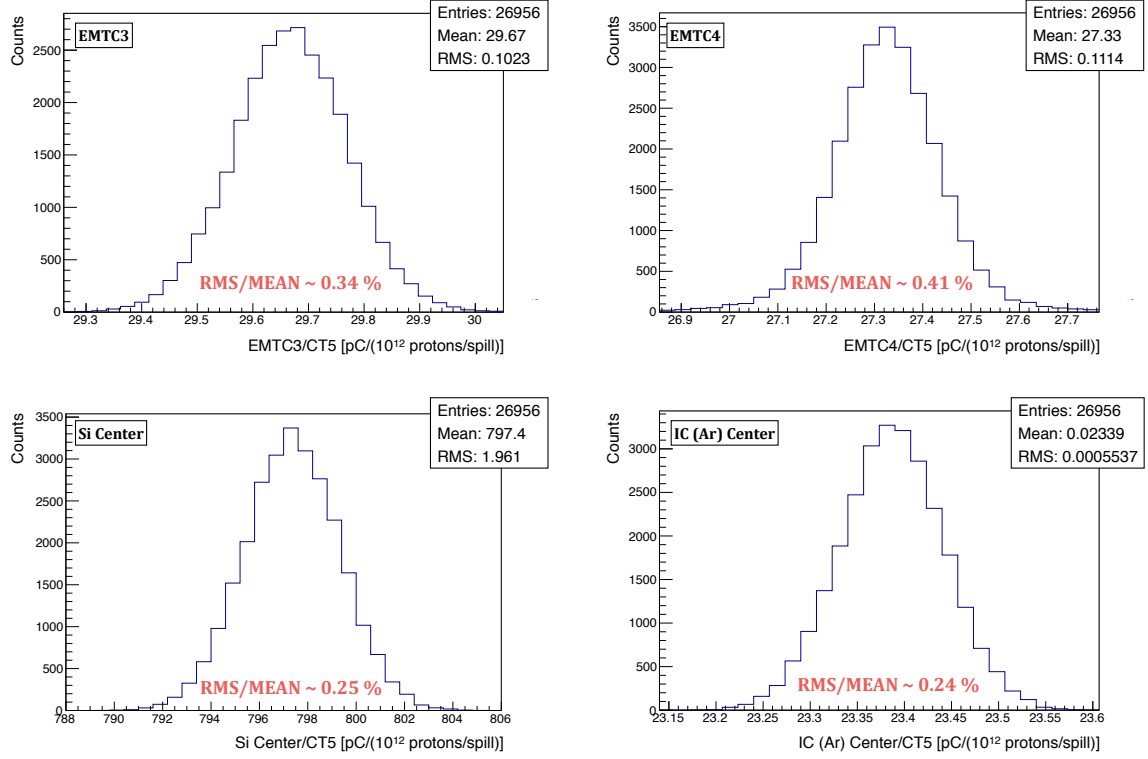


Figure 12: The normalized signal size of EMT3 (top left), C4 (top right), Si center (bottom left), and IC (Ar) center (bottom right) at 450 kW beam power and +250 kA horn current (corresponding to a muon flux of 3.2×10^6 /cm² per 80 ns beam bunch). The intensity resolutions for each sensor type are summarized in Table 3.

Table 3: Summary of the intensity resolution of each detector for spill-by-spill and first bunch measurements. The proton beam intensity is 450 kW and the horn current setting is +250 kA, corresponding to a muon flux of 3.2×10^6 /cm² per 80 ns beam bunch. The statistical uncertainty is less than 0.01%.

Detector	Spill (8 bunch sum)	First bunch
EMTC3	0.34%	0.73%
EMTC4	0.41%	0.78%
Si center	0.25%	0.37%
IC (Ar) center	0.24%	0.33%

5.4. Linearity

A linear sensor response is desired to correctly monitor the beam at low power during beam tuning up to high power during physics operation. In order to test the linearity performance of the EMTs, beam intensity scans were carried out. During scans, the proton beam power was set to 13 kW, 50 kW, 150 kW, 260 kW, 340 kW, 400 kW, 460 kW, and 500 kW, and the horn current setting was +250 kA. Two different voltages were applied to the EMTs to study space charge effects inside the EMT, which occur when the number of produced electrons is so large that the electric field is significantly distorted, causing a decreased signal yield, similar to the IC case described in Section 2. We applied -450 V to reduce the number of secondary electrons, and compared the linearity performance to the case with -500 V applied. The scan conditions are summarized in Table 4.

Table 4: Beam powers and EMT applied voltages during beam intensity scans. Note that the the number of protons per kW at a repetition rate of 2.48 s is 5.3×10^{11} protons/spill/kW.

Scan	Beam power [kW]	Applied HV [V]
I	150, 260, 340, 400, 460	-500
II	260, 340, 400, 460	-450
III	13, 50	$-500, -450$
IV	500	-500

Since the muon yield is correlated with the horn current, a correction to the calculated yield is applied using horn current monitor information. The correction factor was determined based on horn current scans (see Ref. [13] for details about the correction). During the intensity scans, the proton beam position was kept within ± 0.5 cm, monitored by SSEM19 and 18, and the effect on the muon flux by this fluctuation is less than 1%. Therefore, no correction for the proton beam position is needed. The proton beam width changes depending on the beam power, from 2 mm (1.5 mm) at the lowest power to 4.8 mm (4 mm) at the highest power in the horizontal (vertical) direction, which does affect the muon flux. A Monte Carlo (MC) simulation [17] was conducted to estimate the change of the muon flux at the EMT position for various values of the beam width, and the result is shown in Figure 13. The measured yields were corrected by factors determined from the simulation results to extract the expected yields at the nominal beam size (4 mm in both the horizontal and vertical directions). During the beam intensity scan, the beam width values were taken from

SSEM18, since SSEM19 had several unreliable points at very low beam powers, where the beam width was too narrow for the monitor sensitivity and profile reconstruction was therefore not possible. The consistency between SSEM19 and 18 has been confirmed by other, reliable, points. To check the width correction validity, two different beam widths, nominal 2.6 mm (2.2 mm) and 4.2 mm (3.2 mm) for the horizontal (vertical) direction, were used at the 150 kW point ($\sim 80 \times 10^{12}$ protons/spill) in Scan I.

Figure 14 shows the scan results for the Si center channel. Here, Si is selected because IC shows non-linearity as described in Section 2. The plot in the left panel shows the result before the beam width correction, and the plot in the right panel shows that after the correction. The horn current correction is applied for both results. At low intensity, points are more scattered due to a poor signal-to-noise ratio because of the small signal size. Therefore, the linearity at scan points above 100 kW ($\sim 50 \times 10^{12}$ protons/spill) is considered more reliable. It is found that the beam width correction works very well, especially for the 150 kW points ($\sim 80 \times 10^{12}$ protons/spill) in Scan I, where, before the MC correction is applied, the distributions are separated due to the different beam widths. The linearity is stable within $\pm 1\%$ from 100 kW to 500 kW.

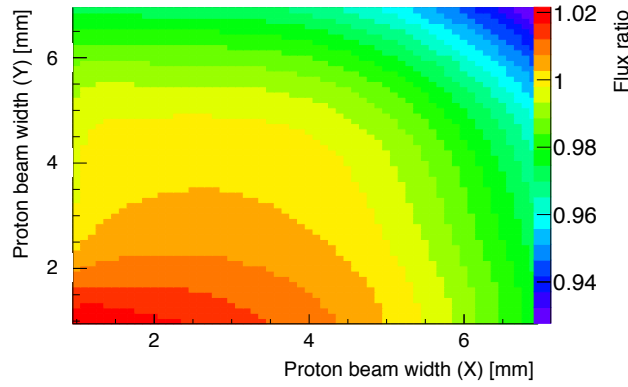


Figure 13: Ratio of the simulated muon flux at the EMT position for various proton beam widths to the simulated muon flux for beam width = (4, 4) mm.

The linearity results for EMTC3 and C4 are shown in Figures 15 and 16, respectively. The results use both horn current and proton beam width corrections. The plots in the left panels show the results with -500 V high voltage (HV) applied, while those in the right panels show the results with -450 V applied. EMTC4 shows better linearity performance than EMTC3, because the capacitance used in the circuit for C4 was improved as described in Section 4. Measurements with lower voltage applied show better linearity, and this indicates that space charge effects exist when a higher voltage is applied. EMTC4 with -450 V applied shows as good linearity as the Si sensor up to 460 kW (muon flux of 3.3×10^6 /cm² per 80 ns beam spill). At higher intensities, non-linearities may appear. To further improve linearity, use of a different dynode divider ratio can be considered, with a possible compromise on signal size.

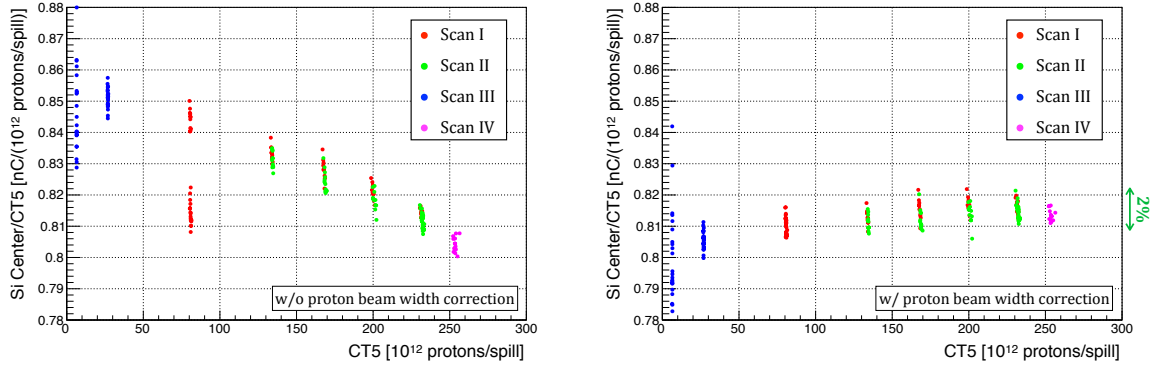


Figure 14: Results of the beam intensity scan for the Si center channel before (left) and after (right) the proton beam width correction. Different colors correspond to different scans, as shown in Table 4.

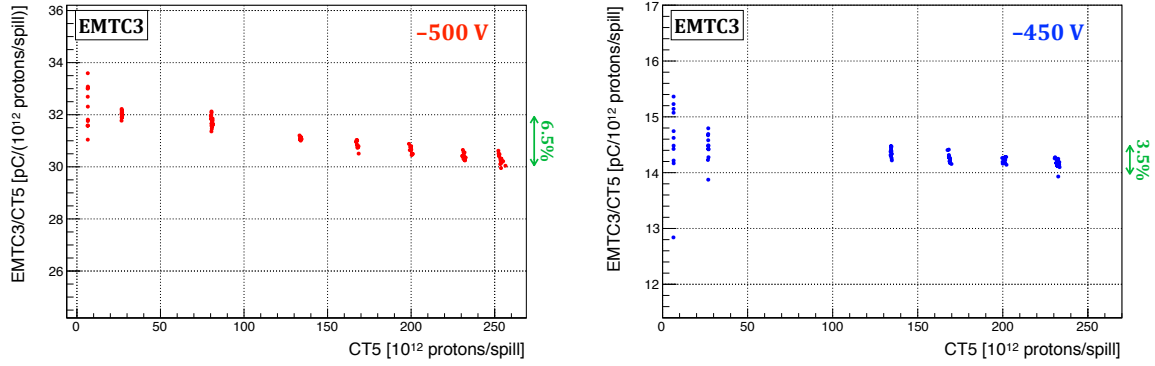


Figure 15: Results of the beam intensity scan for EMT C3. The left panel shows the result with -500 V applied, and the right panel shows the result with -450 V applied.

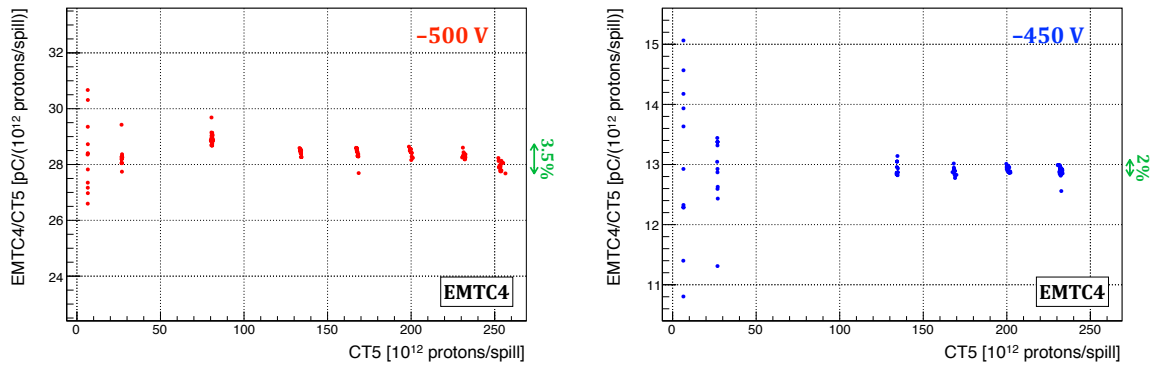


Figure 16: Results of the beam intensity scan for EMT C4. The left panel shows the result with -500 V applied, and the right panel shows the result with -450 V applied.

5.5. Stability

The muon monitor must work stably during continuous running. Yield fluctuations are required to be within 3%. The EMTs were continuously exposed to the T2K muon beam over five data-taking periods. The beam conditions and applied HVs for each period are summarized in Table 5. Periods I and II are separated because EMTC4 was installed between them. EMTC3 was installed before Period I, when several tests, such as HV and attenuation level tuning, were performed. Therefore, the EMTC3 stability during the period before Period I is not shown here. There is an approximately half-year beam-off period between Periods II and III, during which the EMTs’ HVs were turned off. Other than that, we turned off the HV of both EMTs for just one day in the middle of Period V in order to check the stability.

Table 5: Beam conditions and HVs for EMTC3 and C4 during each beam exposure period.

Period	Horn current [kA]	HV [V]	POT [$\times 10^{18}$]
I (23, Feb., 2017 \sim 30, Mar., 2017)	+250	−500	224.1
II (31, Mar., 2017 \sim 12, Apr., 2017)	+250	−500	76.8
III (16, Oct., 2017 \sim 22, Oct., 2017)	+250	−505	20.5
IV (22, Oct., 2017 \sim 2, Nov., 2017)	−250	−505	59.4
V (2, Nov., 2017 \sim 22, Dec., 2017)	−250	−450	305.8

Figures 17, 18, 19, and 20 show the yield versus time for the Si center channel, IC center channel, EMTC3, and EMTC4, respectively. The effect of the horn current on the muon flux is corrected as described in Section 5.4. There are two jumps observed in the EMTC3 signal, the cause of which is still unknown; however, these appear to be synchronized with unrelated IC calibration work. Both EMTC3 and C4 show a drift in the yield following the initial application of HV, in Periods I and III for C3 and Periods II and III for C4. This drift is assumed to be due to the stabilization of the dynode materials, which are generally alkali metals and antimony (Sb). Usually, PMTs require “warming up” by irradiation with light for initial stabilization [15]; however, EMTs cannot be warmed up because they do not have a photocathode. The required warm-up output charge is several μA for several minutes, which is equivalent to several mC. Table 6 shows the integrated charge output by the time the EMT signal yield became stable during our tests. The values are reasonable compared to the expected charge for PMT warm-up. For later runs, both EMTC3 and C4 stabilized after fewer incident POT. This is thought to be due to stabilization of the dynode materials at some level by previous irradiation. After the initial drift period, the yield is basically stable within $\pm 1\%$ excluding some periods where the yield fluctuated due to manually changing the EMT HV or changes in the proton beam conditions. This demonstrates that EMTs fulfill the requirement of $< 3\%$ signal fluctuation.

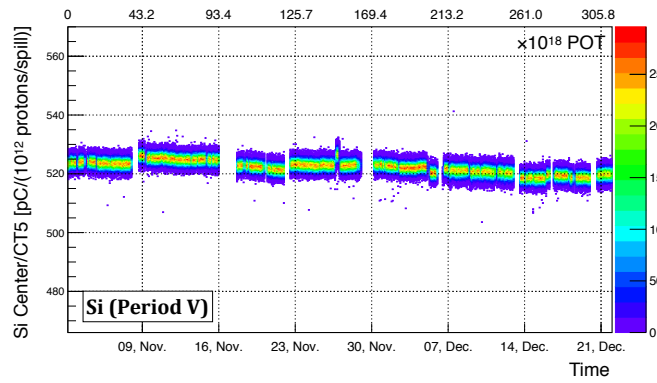
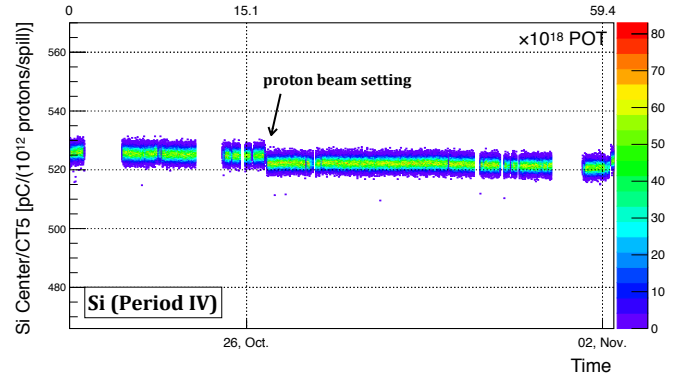
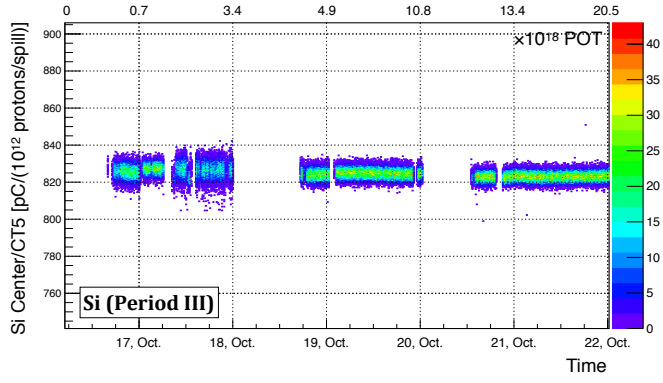
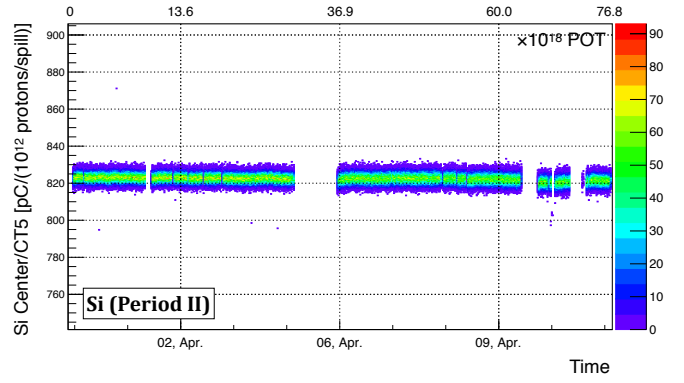
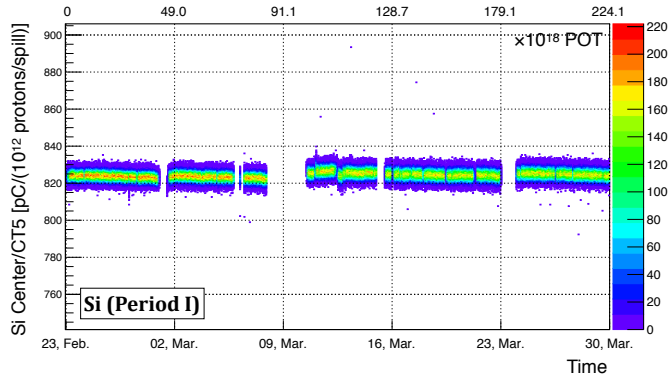


Figure 17: Signal yield of Si center channel as a function of time.

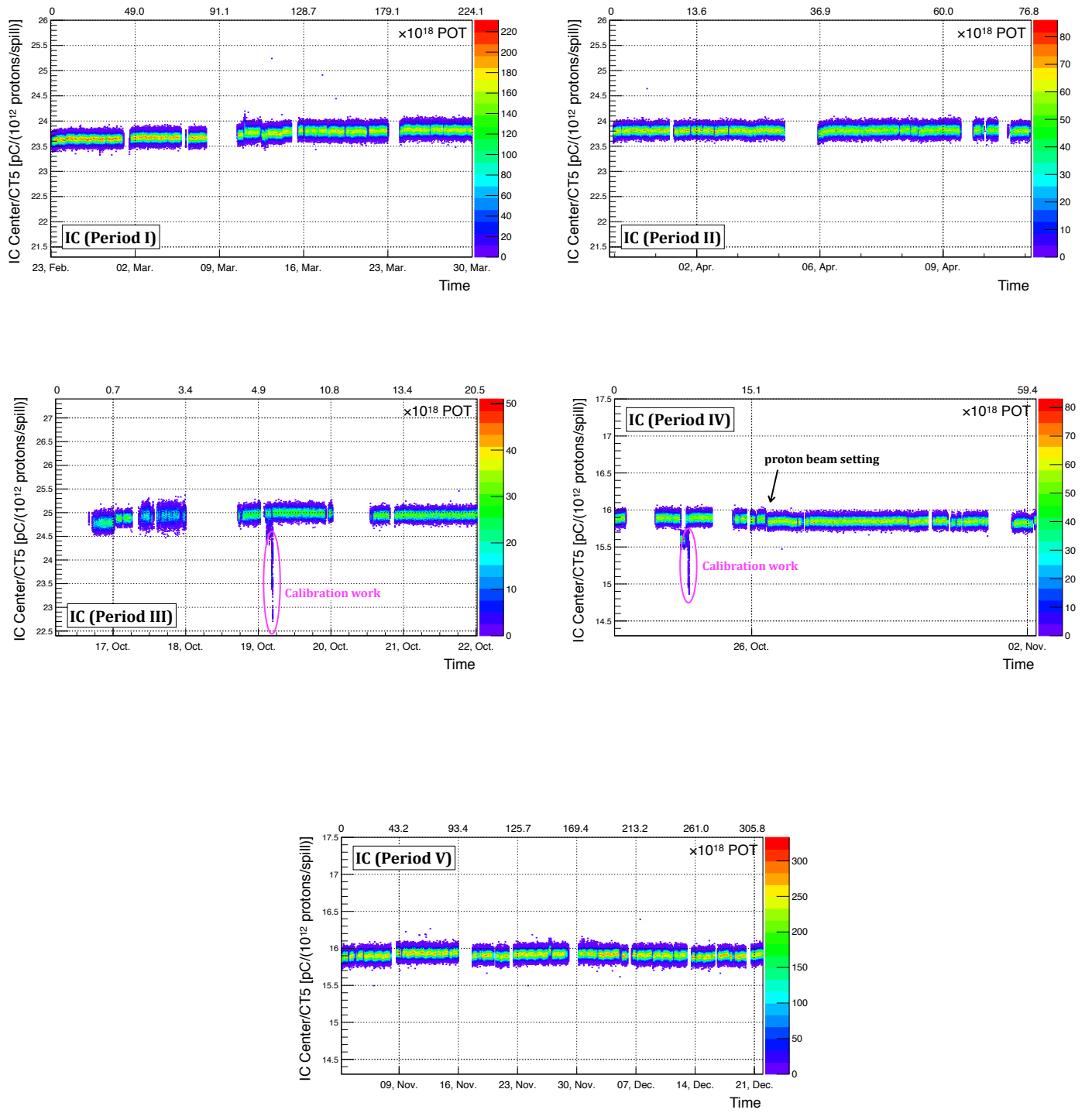


Figure 18: Signal yield of IC (Ar) center channel as a function of time. The yield jumps seen in Periods III and IV, marked with magenta circles, are due to calibration work where the entire IC system was moved (see Ref. [13] for the calibration method).

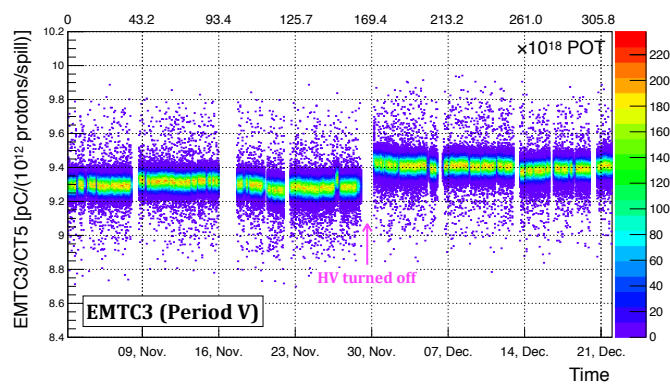
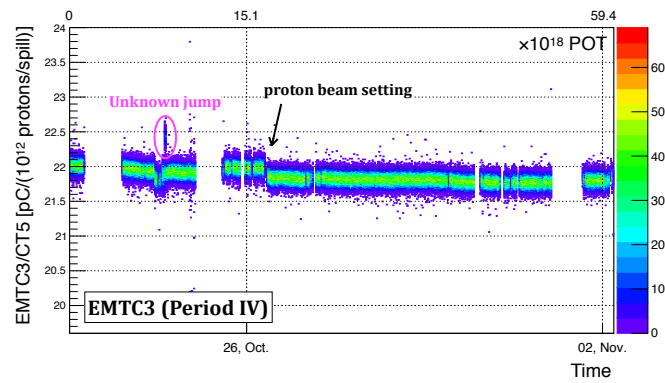
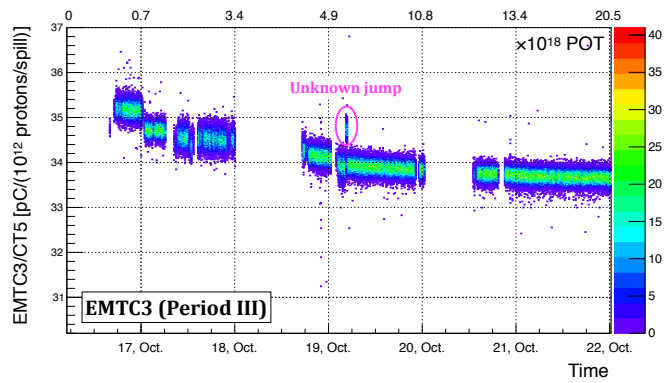
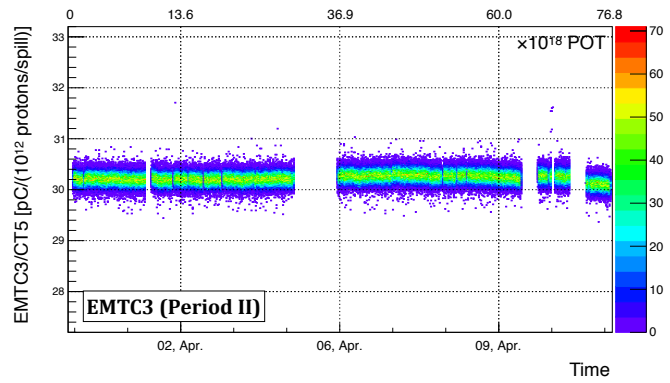
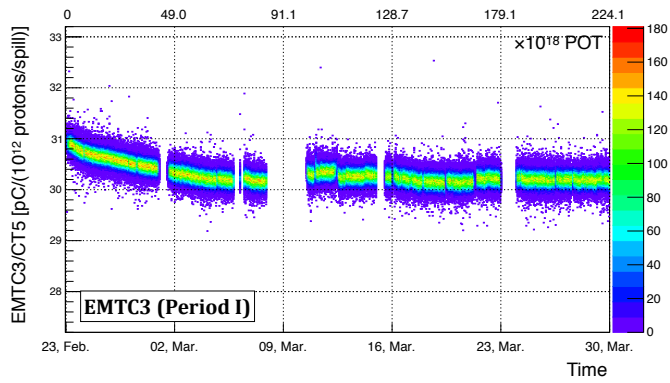


Figure 19: Signal yield of EMTC3 as a function of time. Two yield jumps are seen and seem to be synchronized with IC calibration work, although the cause is not fully understood. After a short HV-off period during Period V, the yield changed.

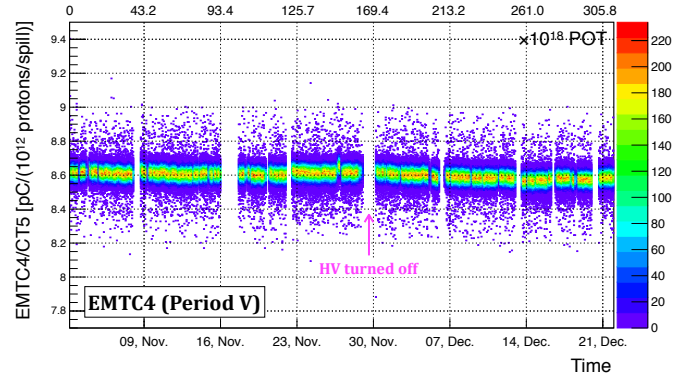
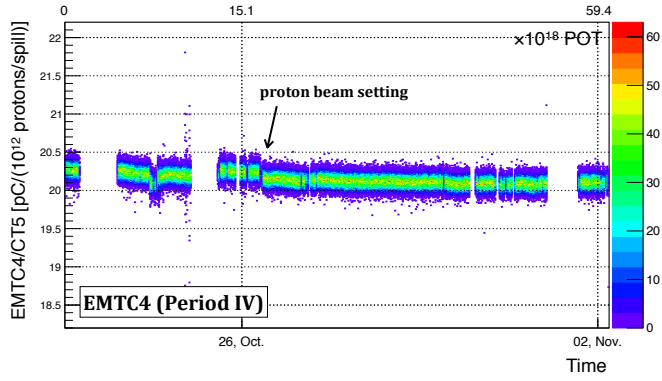
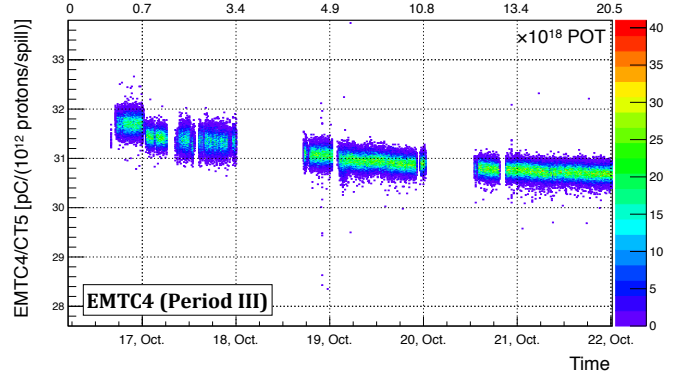
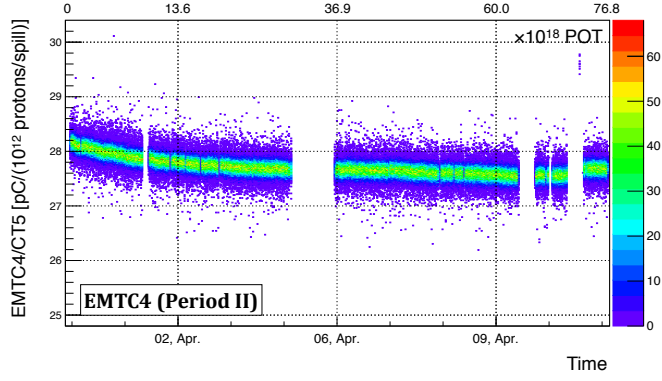


Figure 20: Signal yield of EMTC4 as a function of time. Other than the short periods just after the HV is turned on, C4 shows stable performance.

Table 6: Total integrated charge output prior to EMT signal yield stabilization. The calculations for Period III assume that the charge per POT is increased by a factor of 1.1, since the applied HV is higher (-505 V). The recommended value for stabilization is several mC.

EMT number	Period	POT amount [$\times 10^{18}$]	Integrated charge [mC]
C3	I	~ 70	~ 2.0
	III	~ 13	~ 0.4
C4	II	~ 50	~ 1.3
	III	~ 13	~ 0.4

6. Conclusion

We are developing an electron-multiplier tube as a possible new muon monitor sensor for the T2K experiment. Two prototype detectors were prepared by modifying the resistances and capacitances of the original divider circuits of Hamamatsu-made EMTs, and these sensors were installed in the muon monitor location. Various properties of EMTs were measured using the T2K muon beam. The EMTs' time response was found to be faster than that of the T2K Si or IC sensors, which is of high importance for bunch-by-bunch monitoring. The EMT spill-by-spill intensity resolution at the current T2K operation conditions is better than the 1% requirement. Linearity tests show that the EMT keeps its linearity within $\pm 1\%$ up to 460 kW at +250 kA horn current (corresponding to a muon flux of 3.3×10^6 /cm² per 80 ns beam bunch). The linearity can be further improved by improving the HV divider circuit configuration. The EMT signal yield gradually decreased during initial EMT operation, and then stabilized. One possible reason for this is the conditioning of the EMT dynode materials. This work is the first demonstration of the usage of EMTs for muon beam monitoring, and indicates a strong possibility of practical use in the future. Furthermore, this study suggests that EMTs could have additional applications as general beam detectors for charged particles, with the merit that the gain is easily tunable for compatibility with various beam intensities. To test the EMT performance at T2K future high beam intensities, an electron beam test of the EMTs is currently under consideration.

Acknowledgements

The authors are grateful to the J-PARC accelerator group for supplying a stable beam. This work was partially supported by MEXT KAKENHI Grant Numbers 25105002, 16H06288, 15J01714, and 17J06141.

References

- [1] J. B. M. Pattison, C. A. Ramm, and W. A. Venus, Neutrino Meeting, CERN, Geneva, Switzerland, 13-14 Jan., 1969, proceedings (1969).
- [2] S. Kopp et al., Nucl. Instr. Meth. Phys. Res. A 568, 503-519 (2006).
- [3] K. Abe et al., Nucl. Instr. Meth. Phys. Res. A 659, 106-135 (2011).
- [4] Y. Fukuda et al., Nucl. Instr. Meth. Phys. Res. A 501, 418-462 (2003).
- [5] K. Abe et al., Phys. Rev. Lett., 118, 151801 (2017).
- [6] K. Abe et al., Phys. Rev. D, 96, 092006 (2017).
- [7] A. K. Ichikawa, Nucl. Instr. Meth. Phys. Res. A 690, 27-33 (2012).
- [8] T. Sekiguchi et al., Nucl. Instr. Meth. Phys. Res. A 789, 57-80 (2015).
- [9] K. Abe et al., Nucl. Instr. Meth. Phys. Res. A 694, 211-223 (2012).
- [10] S. Bhadra et al., Nucl. Instr. Meth. Phys. Res. A 703, 45-58 (2013).
- [11] K. Matsuoka et al., Nucl. Instr. Meth. Phys. Res. A 624, 591-600 (2010).
- [12] T. Higuchi et al., Computing in High Energy and Nuclear Physics (2003).
- [13] K. Suzuki et al., Prog. Theor. Exp. Phys., 053C01 (2015).
- [14] K. Abe et al., arXiv:1607.08004 (2016).
- [15] Hamamatsu Photonics K. K., Photomultiplier Tubes Basic and Applications Third Edition (2007).
- [16] R. D. Winn and Y. Onel, Journal of Physics: Conference Series, 404, 012021 (2012).
- [17] K. Abe et al., Phys. Rev. D, 87, 012001 (2013).